# Time keeping and searching for new physics using metastable states of Cu, Ag, and Au

V. A. Dzuba,[1] Saleh O. Allehabi,[1] V. V. Flambaum,[1] Jiguang Li,[2] and S. Schiller[3]
[1]*School of Physics, University of New South Wales, Sydney 2052, Australia*
[2]*Institute of Applied Physics and Computational Mathematics, 6 Huayuan Road, Haidian District, Beijing, China*
[3]*Institut für Experimentalphysik, Heinrich-Heine-Universität Düsseldorf, 40225 Düsseldorf, Germany*

(Received 25 June 2020; accepted 1 February 2021; published 17 February 2021)

We study the prospects of using the electric quadrupole transitions from the ground states of Cu, Ag, and Au to the metastable states $^2D_{5/2}$ as clock transitions in optical lattice clocks. We calculate lifetimes, transition rates, and systematic shifts and find that they are very suitable for this purpose. In particular, the elements are found to have a blackbody radiation shift that is one to two orders smaller than that of Sr. The Au clock is found to have strong sensitivities to a variation of the fine-structure constant, to effects of scalar dark matter, and to a violation of local Lorentz invariance (LLI). Cu and Ag are also suitable for tests of LLI. We identify two more metastable states ($^4F^o_{9/2}$), one in Cu and another in Au, which can serve as additional clock transitions. The $\alpha$-sensitivity coefficients of the two Au clock transitions are large and have opposite sign. This doubles the overall sensitivity to variation of $\alpha$ and opens the possibility of a $\alpha$-variation test with a single neutral atomic species. We also present more accurate or additional values of the sensitivity to local position invariance violation for several established or proposed clock transitions. These values are important for properly evaluating the effectiveness of clock-clock comparisons.

DOI: 10.1103/PhysRevA.103.022822

## I. INTRODUCTION

The use of optical clock transitions for searching for new physics beyond the standard model is a promising area of research. A hypothetical manifestation of new physics at low energy is expected to be very small. Therefore, the highest possible accuracy of the measurements is needed. Fractional uncertainty of the best optical clocks currently is around $1 \times 10^{-18}$ [1–7], allowing for the highest accuracy so far achieved in the history of measurements. However, apart from one exception ($Yb^+$), the best current optical clocks are only weakly sensitive to new physics such as time variation of the fine-structure constant, violation of local position invariance (LPI), and violation of local Lorentz invariance (LLI), etc. [8–11]. LPI, LLI, and the weak equivalence principle form the Einstein equivalence principle, which is the foundation of general relativity.

Several ideas were proposed to combine a high accuracy of optical clocks with a high sensitivity to new physics. These include the use of the highly charged ions (HCIs) [12–15], nuclear clocks [16], and metastable atomic states with a large value of the total angular momentum $J$ ($J > 1$) [8,17–20]. These states are connected to the ground state via transitions, that correspond to single-electron transitions with large change of the single-electron total angular momentum $j$. The large $\Delta j$ is what makes the transition sensitive to the variation of the fine-structure constant (see, e.g., [21]). For example, in the present work, we consider transitions between the $nd^{10}(n+1)s\ ^2S_{1/2}$ ground state and the $nd^9(n+1)s^2\ ^2D_{5/2}$ excited metastable state. This is roughly the $s_{1/2}$ to $d_{5/2}$ transition with $\Delta j = 2$.

The energy diagrams displaying seven low-lying states of Cu and Au and the five lowest states of Ag studied in this work are presented in Fig. 1. One metastable state of interest ($^2D_{5/2}$) is the first-excited state for Cu and Au. In Ag, the $^2P^o_{1/2}$ state lies below the $^2D_{5/2}$ clock state. However, this has no significance since the states are very weakly connected (by $E3$, $M2$, or hyperfine-induced $E1$ transitions with very small value of transition frequency, $\hbar\omega = 690\ \mathrm{cm}^{-1}$). Cu and Au each have another, higher-energy metastable state, $nd^9\,(^2D_{5/2})(n+1)s_{1/2}\,(n+1)p_{3/2}(^3P_2)\,^4F^o_{9/2}$, which can be used in an additional clock transition connecting this state to the $^2D_{5/2}$ clock state via a $M2$, $E3$, or hyperfine-induced $E1$ transition. Having two clock transitions in one atom is a potential important advantage in using clocks for the search of $\alpha$ variation and LPI violation. The Au $^4F$ state has been observed in magnetic resonance experiments on atomic beams [22,23].

The clock transition in Ag was studied experimentally in Ref. [24] under two-photon excitation, not under $E2$ excitation. For an optical clock application, an $E2$ excitation is advantageous compared to a two-photon excitation since the involved laser intensity is much lower, leading to a lower corresponding systematic shift.

The sensitivity of the $^2D_{5/2}$ metastable states of Ag and Au to variation of the fine-structure constant was studied before [8]. In this work, we further study these two, as well as three other metastable states, in terms of their suitability for high-accuracy measurements and sensitivity to other manifestations of new physics, such as LPI violation and LLI violation.

## II. CALCULATIONS

### A. Methods

We are mostly interested in the lowest states of Cu, Ag, and Au shown in Fig. 1. The $D$, $F$, and some $P$ states of

 

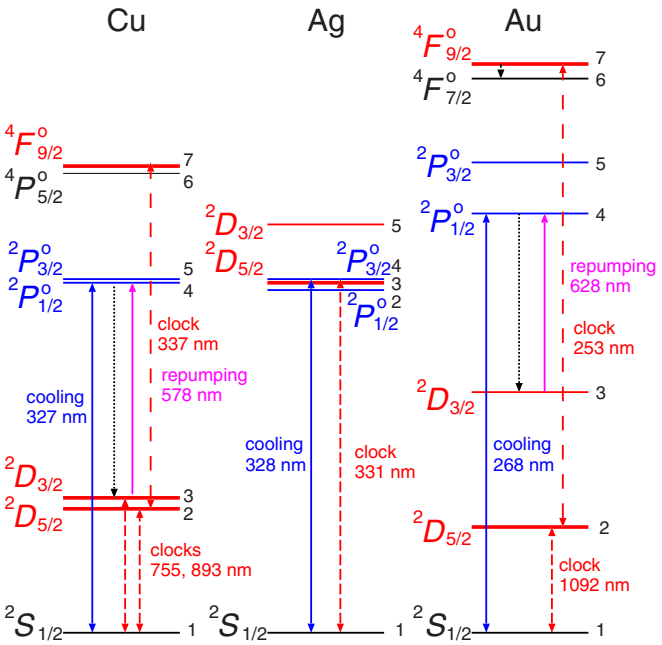


FIG. 1. Energy diagram (approximately to scale) for the lowest states of Cu ($I = 3/2$), Ag ($I = 1/2$), and Au ($I = 3/2$). Thick red lines indicate the upper clock states. Electric quadrupole ($E2$) clock transitions are shown as short-dashed red lines. Additional clock transitions in Cu and Au are shown as long-dashed red lines. Cooling transitions are shown as solid blue lines. The presence of leakage transitions (black dotted lines) implies the need for repumping (magenta lines). Numeration of the states corresponds to the one in Table II.

all three atoms have excitations from a $d$ shell. This means that the $d$ shell is open and $d$ electrons should be treated as valence ones. The total number of valence electrons, i.e., 11, is too large for most standard computational approaches. We use a version of the configuration interaction (CI) method specifically developed for such systems (the CI with perturbation theory (CIPT) method [25]). In this method, off-diagonal matrix elements of the CI Hamiltonian between highly excited states are neglected. This allows one to reduce the CI matrix to an effective matrix of a small size in which the contribution from high states is included perturbatively.

The CI equations can be written in a matrix form via matrix blocks [25,26],

$$\begin{aligned} AX + BY &= EX, \\ CX + DY &= EY, \end{aligned} \tag{1}$$

where $A$ is a matrix of small size containing matrix elements between low-energy states, which dominate in the wave-function expansion, $B$ and $C$ are blocks of the CI matrix containing matrix elements between low and high states ($c_{ij} = b_{ji}$ since the CI matrix is symmetric), $D$ is a diagonal matrix ($d_{ik} = \langle k|H^{\rm CI}|k\rangle\delta_{ik}$), $E$ is an eigenenergy, and $X$ and $Y$ are parts of the eigenvector containing expansion coefficients of the wave function for valence electrons over a set of single-determinant basis functions. From the second equation (1), we get

$$Y = (EI - D)^{-1}CX, \tag{2}$$

where $I$ is the unit matrix. Since $D$ is a diagonal matrix, (2) can be rewritten as

$$y_k = \frac{1}{E - E_k}\sum_m c_{km}x_m, \tag{3}$$

where $E_k = \langle k|H^{\rm CI}|k\rangle$ is the diagonal CI matrix element for high-energy states.

By substituting (2) into (1), we get the CIPT equation,

$$[A + C(EI - D)^{-1}B]X = EX. \tag{4}$$

Once the energy $E$ and the wave function $X$ are found by solving (4), a correction to the wave function $Y$ can be found using (2) and (3). Note that after $Y$ is calculated, the total wave function should be renormalized. This is because the solution of (4) is normalized by $\sum_k x_k^2 = 1$, while the total wave function should be normalized by $\sum_k x_k^2 + \sum_m y_m^2 = 1$.

In our previous works [25,27–31], only the solution of the CIPT equation (4) was implemented, while the correction to the wave function (2) was not calculated. In the present work, we calculate $Y$ too and include it in the calculation of the matrix elements (see below).

We perform the calculations in the $V^{N-1}$ approximation, with one electron removed from the initial relativistic Hartree-Fock (HF) calculations to obtain the potential for calculating single-electron basis states. The B-spline technique [32] is used to construct single-electron basis states above the core. Many-electron states for the CIPT calculations are constructed by exciting one or two electrons from a reference configuration and then using the resulting configurations to build all corresponding many-electron states of definite value of the total angular momentum $J$ and its projection $J_z$. States corresponding to about 100 lowest nonrelativistic configurations go into the effective CI matrix, while higher states are treated perturbatively. Note that our calculations are completely relativistic. We only use nonrelativistic configurations to simplify the procedure of generating many-electron basis states. In the list of nonrelativistic configurations, each of them is subsequently replaced by a corresponding set of relativistic configurations. For example, the $5d^9 6s6p$ configuration is replaced by four relativistic ones, i.e., the $5d^4_{3/2}5d^5_{5/2}6s6p_{1/2}$, $5d^3_{3/2}5d^6_{5/2}6s6p_{1/2}$, $5d^4_{3/2}5d^5_{5/2}6s6p_{3/2}$, and $5d^3_{3/2}5d^6_{5/2}6s6p_{3/2}$ configurations.

To check the stability of the results, we perform calculations in a different way. We keep the minimum number of possible configurations in the effective CI matrix [block $A$ in Eq. (1)], but introduce an extra term into the CI Hamiltonian, i.e., the effective polarization potential,

$$\delta V_l = -\frac{\alpha_l}{a^4 + r^4}. \tag{5}$$

This term imitates the effect of core-valence correlations. Its form is chosen to coincide with the polarization potential ($V_p = -\alpha/r^4$) on large distances. The parameter $a$ is a cutoff parameter introduced to remove the singularity at $r = 0$. We use $a = 1a_B$ and treat $\alpha_l$ as a fitting parameter. Here, $l$ is the value of the angular momentum, indicating that we use different fitting parameters in the calculation of the $s$, $p$, and $d$ single-electron basis states. The values of $\alpha_s$ are chosen to fit ionization potentials (IPs), the values of $\alpha_p$ are chosen to fit the energies of the states of the $nd^{10}(n+1)p$ configuration,

TABLE I. Fitting parameters for the effective polarization potential (5).

| Atom | $\alpha_s$ | $\alpha_p$ | $\alpha_d$ |
|---|---|---|---|
| Cu | 0.72 | 0.88 | 0.22 |
| Ag | 0.71 | 0.81 | 0.24 |
| Au | 0.69 | 0.92 | 0.34 |

and the values of $\alpha_d$ are chosen to fit the energies of the states of the $nd^9(n+1)s^2$ configuration.

### B. Energies

The obtained fitting parameters are presented in Table I. Energy levels, calculated in the two different approaches, are presented in Table II. Note the significant improvement to the energies due to the fitting. The fitting is not perfect because we use one fitting parameter for both components of the fine structure. We do this to avoid a false contribution to the fine structure (e.g., a contribution which does not vanish in the nonrelativistic limit).

Fitting also improves the wave functions, leading to more accurate values of the matrix elements. Comparing transition amplitudes and other matrix elements obtained with and without fitting is an important test of the theoretical uncertainty.

We point out that the fitting can be used for improved predictions of the spectra of systems with poor experimental data, e.g., superheavy elements or highly charged ions. To do so, we need to perform accurate fitting for a system with known spectra and electronic structure similar to the system

TABLE II. Excitation energies ($cm^{-1}$), ionization potential (IP, $cm^{-1}$), and lifetimes for six states of Cu and Au and for the four lowest excited states of Ag. Lifetime values without indicated uncertainties are theoretical values.

| | | | Energy ($cm^{-1}$) | | | Lifetime | |
|---|---|---|---|---|---|---|---|
| | | | NIST | Present work | | Present | |
| $N$ | Conf. | Term | [53] | No fitting | Fitted | work | Other |
| | | | | Cu | | | |
| 1 | $3d^{10}4s$ | $^2S_{1/2}$ | 0 | 0 | 0 | $\infty$ | |
| 2 | $3d^94s^2$ | $^2D_{5/2}$ | 11203 | 10521 | 11277 | 45 s | 26.76 s[a] |
| 3 | $3d^94s^2$ | $^2D_{3/2}$ | 13245 | 12270 | 13331 | 7.3 s | 4.46 s[a] |
| 4 | $3d^{10}4p$ | $^2P^o_{1/2}$ | 30535 | 29489 | 30513 | 7.1 ns | 7.4(2) ns[b] |
| | | | | | | | 6.535 ns[a] |
| 5 | $3d^{10}4p$ | $^2P^o_{3/2}$ | 30784 | 31115 | 30772 | 6.9 ns | 7.1(2) ns[b] |
| | | | | | | | 6.369 ns[a] |
| 6 | $3d^94s4p$ | $^4P^o_{5/2}$ | 39018 | 38693 | | | |
| 7 | $3d^94s4p$ | $^4F^o_{9/2}$ | 40909 | 40400 | | 600 s | 6897 s[a] |
| IP | $3d^{10}$ | $^1S_0$ | 62317 | 60328 | 62333 | | |
| | | | | Ag | | | |
| 1 | $4d^{10}5s$ | $^2S_{1/2}$ | 0 | 0 | 0 | $\infty$ | |
| 2 | $4d^{10}5p$ | $^2P^o_{1/2}$ | 29552 | 29495 | 29549 | 6.6 ns | 7.41(4) ns[c] |
| | | | | | | | 6.85 ns[a] |
| 3 | $4d^95s^2$ | $^2D_{5/2}$ | 30242 | 32480 | 30289 | 0.26 s | 0.2 s[d] |
| 4 | $4d^{10}5p$ | $^2P^o_{3/2}$ | 30473 | 30451 | 30437 | 6.1 ns | 6.79(3) ns[c] |
| | | | | | | | 6.25 ns[a] |
| 5 | $4d^95s^2$ | $^2D_{3/2}$ | 34714 | 36430 | 34804 | 79 $\mu$s | 40 $\mu$s[e] |
| | | | | | | | 65.8 $\mu$s[a] |
| IP | $4d^{10}$ | $^1S_0$ | 61106 | 58891 | 61141 | | |
| | | | | Au | | | |
| 1 | $5d^{10}6s$ | $^2S_{1/2}$ | 0 | 0 | 0 | $\infty$ | |
| 2 | $5d^96s^2$ | $^2D_{5/2}$ | 9161 | 10670 | 9161 | 44 s | |
| 3 | $5d^96s^2$ | $^2D_{3/2}$ | 21435 | 22096 | 21744 | 33 ms | |
| 4 | $5d^{10}6p$ | $^2P^o_{1/2}$ | 37359 | 38853 | 36784 | 4.1 ns | 6.0(1) ns[b] |
| 5 | $5d^{10}6p$ | $^2P^o_{3/2}$ | 41175 | 43028 | 41217 | 3.3 ns | 4.6(2) ns[b] |
| 6 | $5d^96s6p$ | $^4F^o_{7/2}$ | 45537 | 46375 | | | |
| 7 | $5d^96s6p$ | $^4F^o_{9/2}$ | 48697 | 49166 | | 2 s | |
| IP | $5d^{10}$ | $^1S_0$ | 74408 | 72806 | 74472 | | |

[a]Reference [34].
[b]Reference [35].
[c]Reference [36].
[d]Extrapolation from $Hg^+$; see Ref. [37] and references therein.
[e]Reference [38].

of interest. Then the same fitting parameters can be used to calculate the unknown spectra.

### C. Transition amplitudes

To calculate transition amplitudes, we use the well-known random phase approximation (RPA; see, e.g., [33]). The RPA equations for a single-electron state have the form

$$(H^{\rm HF} - \epsilon_c)\delta\psi_c = -\big(\hat{F} + \delta V_F^{N-1}\big)\psi_c. \tag{6}$$

Here, $H^{\rm HF}$ is the relativistic Hartree-Fock Hamiltonian, the index $c$ numerates single-electron states, $\hat{F}$ is the operator of an external field, $\delta\psi_c$ is a correction to the state $c$ due to an external field, and $\delta V_F^{N-1}$ is the correction to the self-consistent Hartree-Fock potential due to the external field. The same $V^{N-1}$ potential is used in the RPA and HF calculations. The RPA equations (6) are solved self-consistently for all states $c$ in the core. Transition amplitudes are found as matrix elements between many-electron states found in the CIPT calculations for the effective operator of an external field,

$$A_{ab} = \langle b|\hat{F} + \delta V_F^{\rm core}|a\rangle. \tag{7}$$

Here, $|a\rangle$ and $|b\rangle$ are many-electron wave functions. They have a form

$$|a\rangle = \sum_k x_k \Phi_k \tag{8}$$

or

$$|a\rangle = \sum_k x_k \Phi_k + \sum_m y_m \Phi_m, \tag{9}$$

where $\Phi_k$ is a single-determinant many-electron basis wave function, $x_k$ comes from the solution of (4), and $y_k$ comes from (3). In our previous works [25,27–31], we used (8), while in the present work, we also include the correction to the wave function (3) and so use (9) for matrix elements. The difference in matrix element values (7) when using (8) or (9) is usually a few percent. In most cases, it does not exceed 2%.

The rates of spontaneous emission are given in atomic units by

$$\Gamma_{E1,M1} = \frac{4}{3}(\alpha\omega)^3 \frac{A^2_{E1,M1}}{2J+1}, \tag{10}$$

for electric dipole ($E1$) and magnetic dipole ($M1$) transitions, and by

$$\Gamma_{E2,M2} = \frac{1}{15}(\alpha\omega)^5 \frac{A^2_{E2,M2}}{2J+1} \tag{11}$$

for electric quadrupole ($E2$) and magnetic quadrupole ($M2$) transitions. In these formulas, $\alpha$ is the fine-structure constant, $\omega$ is the energy difference between the lower and upper states, $A$ is the amplitude of the transition (7), and $J$ is the total angular momentum of the upper state. The magnetic amplitudes $A_{M1}$ and $A_{M2}$ are proportional to the Bohr magneton, $\mu_B = |e|\hbar/2mc$. Its numerical value in Gaussian-based atomic units is $\mu_B = \alpha/2 \approx 3.65 \times 10^{-3}$. The lifetimes of the excited states are calculated by $\tau_a = 2.4189 \times 10^{-17}/\sum_b \Gamma_{ab}$, where $\tau_a$ is the lifetime of atomic state $a$ in seconds, the summation goes over all possible transitions to lower states $b$, and the transition probabilities $\Gamma_{ab}$ are given by (10) or (11). Lifetimes were calculated using the transition amplitudes and probabilities reported in Table III. The lifetimes of the lowest states of Cu, Ag, and Au are presented in Table II.

Table III presents the amplitudes calculated in the first approach (large CI matrix and no fitting). The difference between the two approaches is a few percent for large amplitudes and up to a few tens of percent for small amplitudes, e.g., amplitudes which vanish in the nonrelativistic limit. Another way to estimate the accuracy of the amplitude calculations is to compare with available experimental data or other calculations, in particular the calculations for Cu and Ag performed with the use of Cowan's code [34]. This is done in Tables II and III. One can see that the accuracy for the calculated amplitudes goes down while moving from Cu to Au, coming to about 50% disagreement with the reference data for a large transition rate in Au for the $E1$ transition between states 4 and 1; see Table III (this translates into about 25% uncertainty in the transition amplitude). For weak transitions, the disagreement might be even larger. The accuracy is better for Cu and Ag. The limited accuracy for the calculated amplitudes is due to the small size of the effective CI matrix. At the present stage, the contribution of the high-energy states is included for the energies, but not for the transition amplitudes. However, the present accuracy is sufficient for the main conclusions of the paper regarding the suitability of the clock states for time keeping and the search for new physics.

It should be mentioned that states with no excitation from the upper $d$ shell (e.g., the $5f^{10}6p_{1/2,3/2}$ states of Au) can be treated more accurately within different approaches, for example, with the use of the correlation potential method [33]. The main advantage of the current approach is that it can be used for any state of the considered atoms, including states with excitations from the upper $d$ shell where most other methods would not work.

## III. ANALYSIS

### A. Clock transitions

Cu has three long-lived metastable states ($N = 2, 3, 7$ in Table II), Ag has one ($N = 4$), and Au has two ($N = 2, 7$). The states of Cu and Au have lifetimes that are substantially larger than 1 s, comparable to those of the currently used Sr and Yb lattice clocks. The 0.2 s lifetime of the Ag upper clock state is comparatively small. Nevertheless, the natural $Q$ factor, $1 \times 10^{15}$, is pronouncedly high and could permit a lattice clock of excellent stability. In the following, we consider the clock transitions between these six states and their respective lower clock states. Note that the two $^2D$ clock states of Cu are very similar and therefore, in most cases, we present the data for only the $^2D_{5/2}$ state. We also do not present a comprehensive analysis for the $^4F^o_{9/2}$ states of Cu and Au, limiting the present work to calculating the lifetimes and sensitivity to new physics.

### B. Laser cooling of Cu, Ag, and Au

#### *1. Silver*

Silver has been laser cooled [42]. Here, the cooling scheme is straightforward: the cooling transition is between the ground and second-excited state, $^2S_{1/2} \to {}^2P_{3/2}$, with only

TABLE III. Transition amplitudes and probabilities for transitions between the seven states of Cu and Au and between the five lowest states of Ag.

| Transition | Type | $\hbar\omega$ ($cm^{-1}$) | This work | | NIST |
|---|---|---|---|---|---|
| | | | $\lvert A\rvert$ (a.u.) | $\Gamma$ ($s^{-1}$) | $\Gamma$ ($s^{-1}$) |
| | | | Cu | | |
| 2-1 | $E2$ | 11203 | 2.603 | 2.23[−2] | |
| 3-1 | $M1$ | 13245 | $0.0002\mu_B$ | 6.27[−7] | |
| 4-1 | $E1$ | 30535 | 2.217 | 1.42[8] | 1.376(14)[8][a] |
| 5-1 | $E1$ | 30784 | 3.140 | 1.45[8] | 1.395(14)[8][a] |
| 3-2 | $M1$ | 2043 | $1.549\mu_B$ | 0.138 | |
| 5-2 | $E1$ | 19581 | 0.546 | 1.13[6] | 2.0(4)[6][b] |
| 4-3 | $E1$ | 17290 | 0.404 | 8.48[6] | 1.65(30)(2)[6][b] |
| 5-3 | $E1$ | 17538 | 0.174 | 8.23[4] | 2.4(4)[5][b] |
| 5-4 | $M1$ | 248 | $1.154\mu_B$ | 1.38[−4] | |
| 7-6 | $E2$ | 1891 | 24.1 | 1.6[−4] | |
| | | | Ag | | |
| 2-1 | $E1$ | 29552 | 2.534 | 1.68[8] | 1.3(1)[8][c] |
| 3-1 | $E2$ | 30242 | 2.872 | 3.90 | |
| 4-1 | $E1$ | 30473 | 3.578 | 1.84[8] | 1.4(1)[8][c] |
| 5-1 | $M1$ | 34714 | $0.00015\mu_B$ | 6.4[−6] | |
| 4-2 | $M1$ | 921 | $1.146\mu_B$ | 6.9[−3] | |
| 5-2 | $E1$ | 5162 | 0.406 | 1.15[4] | |
| 4-3 | $E1$ | 230 | 0.534 | 1.75 | 1.6(6)[d] |
| 5-3 | $M1$ | 4472 | $1.536\mu_B$ | 1.42 | |
| 5-4 | $E1$ | 4242 | 0.175 | 1.18[3] | |
| | | | Au | | |
| 2-1 | $E2$ | 9161 | 4.359 | 2.29[−2] | |
| 3-1 | $M1$ | 21435 | $0.0008\mu_B$ | 4.25[−5] | |
| 4-1 | $E1$ | 37359 | 2.153 | 2.45[8] | 1.64(3)[8][e] |
| 5-1 | $E1$ | 41175 | 2.923 | 3.02[8] | 1.98(14)[8][e] |
| 3-2 | $M1$ | 12274 | $1.549\mu_B$ | 29.9 | |
| 5-2 | $E1$ | 32013 | 0.983 | 1.61[6] | 1.90(13)[7][e] |
| 4-3 | $E1$ | 15924 | 0.504 | 1.04[6] | 3.4(1.7)[6][e] |
| 5-3 | $E1$ | 19739 | 0.243 | 2.30[5] | 5.2(2.6)[5][e] |
| 5-4 | $M1$ | 3816 | $1.141\mu_B$ | 0.488 | |
| 7-6 | $M1$ | 3160 | $2.4\mu_B$ | 5.1[−1] | |

[a]Reference [39].
[b]Reference [40].
[c]Reference [41].
[d]Reference [42].
[e]Reference [35].

weak leakage to the clock state 3. A repumper laser is nevertheless needed because of the small hyperfine splitting in the excited state.

#### 2. Gold

A scheme for laser cooling of Au is presented in Fig. 2. The main cooling transition is the electric dipole transition between the ground state and the excited odd-parity $^2P^o_{1/2}$ state. Compared to using $^2P^o_{3/2}$ as the upper level, the advantage is that only one repumper is needed and that the longer cooling wavelength is experimentally advantageous. There is leakage from the $^2P^o_{1/2}$ to the $^2D_{3/2}$ state by another electric dipole transition ($4 \rightarrow 3$). Therefore, without repumping, only ∼250 cycles are possible. With repumping (628 nm), the cooling may go for as long as needed. Another leakage channel is too weak to affect the scheme.

#### 3. Copper

A cooling scheme similar to silver can be considered for copper: $^2S_{1/2} \rightarrow {}^2P_{1/2}$. It requires one additional laser for repumping.

#### 4. Additional remarks

Optical lattice clocks require the cooling of atoms to the $\mu$K level for efficient loading of the optical lattice with the atoms. Therefore, after cooling on the strong $E1$ transition to a temperature of the order of 1 mK, a second cooling process utilizing a weak transition should follow ("narrow-linewidth cooling"). One option is to cool on the $^2S_{1/2} \rightarrow {}^2D_{3/2}$

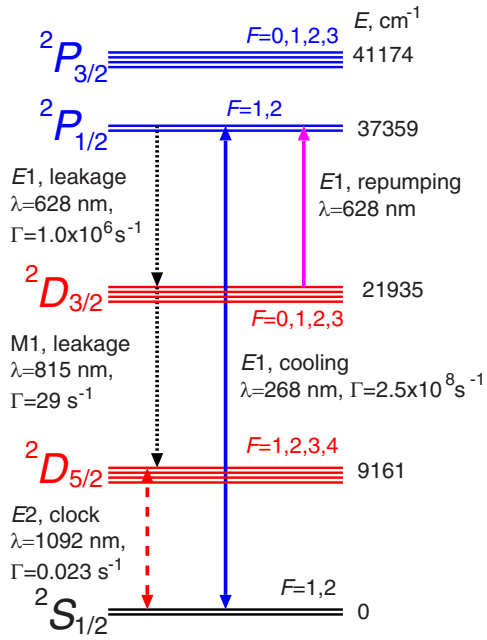


FIG. 2. Details of the level scheme of $^{197}$Au ($I = 3/2$) (not to scale) with proposed laser cooling. The hyperfine structure is shown schematically. The magenta arrow shows the repumper transition. Narrow-linewidth laser cooling is not shown. The clock transition (dashed red line) is composed of several hyperfine components.

transition (1-3 for Cu, 1-5 for Ag, 1-3 for Au). These are $M1$ transitions and are very weak. However, the strengths could be increased and the lifetime of the $^2D_{3/2}$ states shortened by $E1$ coupling them to the respective $^2P$ states using appropriate laser waves. The 1-5 transition in Ag might be directly usable for narrow-linewidth cooling. This transition has been observed under two-photon excitation [38].

The hyperfine structure in both lower and upper laser cooling levels will typically require additional repumper fields to optimize cooling efficiency (see above). We shall not discuss such experimental details here.

Finally, we note that copper and silver atoms have been cooled using buffer-gas cooling [43].

### C. Polarizabilities, blackbody radiation shifts, and magic frequencies

Knowledge of the atomic polarizabilities for both states of the clock transition is important for estimation of the frequency shift caused by blackbody radiation and for finding the *magic* frequency of the lattice laser field, i.e., the frequency at which the dynamic polarizabilities of both states are equal, causing no frequency shift.

The static scalar polarizability $\alpha_v(0)$ of an atom in state $v$ is given by

$$\alpha_v(0) = \frac{2}{3(2J_v+1)} \sum_n \frac{|\langle v||D||n\rangle|^2}{E_n - E_v}, \tag{12}$$

where $D$ is the electric dipole operator with the RPA correction (see the previous section), and the summation goes over the complete set of excited many-electron states.

Static scalar polarizabilities of the ground states of Cu, Ag, and Au are known from a number of calculations and measurements [44]. Table IV presents the recommended values taken from Ref. [44]. In contrast, to the best of our knowledge, there is no similar data for the upper clock states of Cu, Ag, and Au. Therefore, we performed the calculations using two different approaches.

In the first approach, we stay within the CIPT method and calculate 20 odd-parity states for each value of the total angular momentum $J$, which satisfies the electric dipole selection rules for the transitions from the ground and clock states ($J = 1/2, 3/2, 5/2, 7/2$). Then we use formula (12) to perform the calculations for both states. These calculations show three important things: (a) there is good agreement with other data for the ground state, (b) there is good saturation of the summation in Eq. (12), (c) the summation for the clock states is strongly dominated by the transitions to the states of the $5d^9 6s6p$ configuration (we use the Au atom as an example).

The last fact implies that a different approach can be used, previously suggested for atoms with open $f$ shells [46]. In this second approach, we use the fact that the sum (12) is dominated by the $6s$-$6p$ transitions, while the open $5d^9$ subshell remains unchanged. Therefore, the open $d$ shell is attributed to the core and treated as a closed shell with an occupational number of 0.9. The atom is treated as a system with two external electrons above the closed-shell core and an appropriate CI+ MBPT (many-body perturbation theory) [47] method is used (see Ref. [46] for more details). The advantage of this approach is the efficient completeness of the basis with two-electron excitations. The shortcoming is the omission of the transition amplitudes involving excitations from the $d$ shell. In contrast, the CIPT approach includes all amplitudes; however, the summation in Eq. (12) is truncated much earlier.

In the end, both approaches give similar results. The results for the clock states are presented in Table IV together

TABLE IV. Scalar static polarizabilities (in $a_B^3$) and BBR frequency shifts for three clock transitions of Cu, Ag, and Au. $\Delta\alpha$ is the difference between the theoretical value for the upper clock state and the experimental value of the lower clock state.

| | $\alpha_g(0)$ | | | $\alpha_c(0)$ | | | | BBR ($T = 300$ K) | |
|---|---|---|---|---|---|---|---|---|---|
| Atom | Expt. [44] | CIPT | CI+MBPT | CIPT | CI+MBPT | Final | $\Delta\alpha$ | $\Delta\nu$ (Hz) | $\Delta\nu/\nu$ |
| Cu[a] | 47(1) | 54.5 | 43.5 | 46.8 | 42.9 | 45(11) | 2(11) | <0.12 | $<3.4\times10^{-16}$ |
| Ag | 55(8) | 51.8 | 50.6 | 45.9 | 49.5 | 47(2) | −8(8) | <0.14 | $<1.5\times10^{-17}$ |
| Au | 36(3) | 35.7 | 34.0 | 38.9 | 33.2 | 36(3) | 0(4) | <0.03 | $<5.6\times10^{-17}$ |

[a]State $c$ is the $^2D_{5/2}$ clock state.

with experimental or estimated theory uncertainties. For these estimations, we used a comparison of the two approaches for the clock states as well as a comparison of the CIPT and CI+MBPT calculations with other data for the ground states.

The results of the calculations indicate that the values of the polarizabilities of the clock states of Cu, Ag, and Au are similar to those of the ground state. This is a nonstandard situation. More often, the polarizabilities of excited states are larger. Indeed, the higher is the state on the energy scale, the smaller is the energy denominator in Eq. (12). The present results can be explained by the fact that the summation in Eq. (12) is dominated by the states of the $5d^{10}np$ configurations for the ground state (we use Au again as an example) and by the states of the $5d^9 6s6p$ configuration for the clock state. The latter states are higher on the energy scale.

The blackbody radiation (BBR) shift is given by (see, e.g., [48])

$$\delta\nu_{\rm BBR} = -\tfrac{2}{15}(\alpha\pi)^3 T^4[\alpha_c(0) - \alpha_g(0)], \tag{13}$$

where $\alpha$ is the fine-structure constant, $T$ is the temperature, and $\alpha_c(0)$ and $\alpha_g(0)$ are static scalar polarizabilities of the clock and ground states, respectively. For simplicity, we do not include the dynamic correction to the BBR shift. For the more complete formula, see, e.g., [48].

The similarity of the polarizabilities implies a substantial cancellation of the blackbody radiation (BBR) frequency shift, a very favorable effect. The total uncertainty of the polarizability difference $\Delta\alpha$ has been evaluated as $u_{\rm tot}^2 = u_{\rm exp}[\alpha_g(0)]^2 + \delta_{\rm theor}^2$, where $\delta_{\rm theor} = \alpha_c(0)_{\rm CIPT} - \alpha_c(0)_{\rm CI+MBPT}$. Since for the three species the difference between experimental values for the ground state and the mean of the two theory results for the upper clock state is smaller or similar to the estimated uncertainty $u_{\rm tot}$, we can only give the upper bounds for the BBR shifts. The results are presented in Table IV. These bounds of the three species are significantly lower than the BBR shifts in the established strontium and ytterbium optical lattice clocks, i.e., $(-53, -25) \times 10^{-16}$, respectively [49,50]. The bound for Ag is actually 100 times lower than the BBR shift of Sr. The bounds of Ag and Au are also smaller than the shift in the mercury lattice clock, $-1.6 \times 10^{-16}$, and the theoretical shift of the recently proposed 431 nm transition in Yb ($-2.9 \times 10^{-16}$ [19]), listed in Table VIII.

More accurate estimations of the BBR shift might be possible if the polarizabilities are measured or calculated to higher accuracy.

Magic frequencies can be found in the vicinity of every resonance for one of the polarizabilities, i.e., when the frequency of the lattice laser field is approximately equal to the excitation energy [energy denominator in Eq. (12)]. The first magic frequency is near the first resonance for the ground-state polarizability, i.e., $\hbar\omega_m \simeq 30\,535$ cm$^{-1}$ (327 nm) for Cu, $\hbar\omega_m \simeq 29\,552$ cm$^{-1}$ (338 nm) for Ag, and $\hbar\omega_m \simeq 37\,359$ cm$^{-1}$ (267 nm) for Au. Note that since the clock states have large values of the total angular momentum ($J = 5/2$), the magic frequencies would also depend on the quadrupole contribution to the polarizabilities. The current level of computational accuracy does not allow one to find accurate values of the magic frequencies. Having more experimental data may help. In the vicinity of a resonance or a few resonances, a semiempirical formula can be used,

$$\alpha_a(\omega) \approx \alpha'_a(0) + \frac{2}{3(2J_v+1)} \sum_b \frac{A_{ab}^2}{\omega - \Delta E_{ab}}, \tag{14}$$

where $\alpha'_a(0)$ is chosen in such a way that $\alpha_a(\omega = 0)$ is equal to the known (e.g., experimental) static polarizability of state $a$. Summation in Eq. (14) goes over close resonances. If the static polarizability is known to sufficient accuracy and amplitudes $A_{ab}$ of $E1$ transitions are extracted from experimental data or from accurate atomic calculations, then (14) can be used to find magic frequencies.

### D. Stark, quadrupole, and Zeeman shifts

The interaction of atomic electrons with an external electric field and its gradient leads to Stark and electric quadrupole shifts of transition frequencies. These shifts are tiny in optical lattice clocks. We consider the shifts in more detail in Appendix A.

The linear Zeeman shift is given by the expression

$$\Delta E_{F,F_z} = g_F \mu_B B F_z, \tag{15}$$

where $g_F$ is the $g$ factor of a particular hyperfine-structure (hfs) state. It is related to the electron $g_J$ factor by

$$g_F = g_J \langle F, F_z = F, I, J|\hat{J}_z|F, F_z = F, I, J\rangle/F. \tag{16}$$

Electron $g$ factors have approximate values $g_{1/2} \approx 2$, $g_{3/2} \approx 0.8$, and $g_{5/2} \approx 1.2$. More accurate values for Cu, Ag, and Au can be found in the NIST tables [53]. For a clock state with $J = 5/2$ and $F = 2$, we have $g_2 = (11/12)g_{5/2} = 1.1$. For a clock state with $J = 3/2$ and $F = 2$, we have $g_2 = (1/2)g_{3/2} = 0.4$.

The linear Zeeman shift can be avoided if only transitions between states with $F_z = 0$ are considered, as suggested in the past for clock operation. Alternatively, one can average over the transition frequencies with positive and negative $F_z$ in order to cancel the linear shift. However, the large individual shifts will make it difficult to achieve an accurate cancellation.

A second-order Zeeman shift is unavoidable. Therefore, it is important to know its value. If we consider transitions between definite hfs components, then the shift is strongly dominated by transitions within the same hfs multiplet. The total shift is the difference between the second-order shifts in the clock and in the ground state. Both shifts are given by

$$\delta E_{F,F_z} = \sum_{F'=F\pm1,F'_z} \frac{|\langle F'F'_zIJ|\hat{J}_z|FF_zIJ\rangle g_J \mu_B B_0|^2}{\Delta E_{\rm hfs}(F,F')}. \tag{17}$$

Here, $\Delta E_{\rm hfs}(F,F') = E(F\,I\,J) - E(F'\,I\,J)$ is the hfs interval. It has a different sign depending on whether this is an up or down transition.

It follows from (B1) that

$$\Delta E_{\rm hfs}(F,F+1) = -A(F+1) - B[2(F+1)^2 + 1 - 2J(J+1) - 2I(I+1)]$$

and

$$\Delta E_{\rm hfs}(F,F-1) = AF + B[2F^2 + 1 - 2J(J+1) - 2I(I+1)].$$

TABLE V. Magnetic dipole ($A$) and electric quadrupole ($B$) hfs constants (MHz) used in the calculation of the second-order Zeeman shift. Values are rounded to 0.1 MHz or to the last significant digit.

| Atom | Ground state | | Clock state | | | Reference |
|---|---|---|---|---|---|---|
| | | $A$ | $A$ | $B$ | | |
| $^{63}$Cu | $^2S_{1/2}$ | 5866.9 | $^2D_{5/2}$ | 749.1 | 186.0 | [51,52,65] |
| $^{63}$Cu | $^2S_{1/2}$ | 5866.9 | $^2D_{3/2}$ | 1851.0 | 137.4 | [51,52,65] |
| $^{107}$Ag | $^2S_{1/2}$ | −1712.5 | $^2D_{5/2}$ | −126 | | [24,57] |
| $^{197}$Au | $^2S_{1/2}$ | 3049.7 | $^2D_{5/2}$ | 80.2 | −1049.8 | [22,57] |

Using experimental values for $A$ and $B$ (see Table V), we calculate the second-order Zeeman shift for Cu, Ag, and Au. The results are presented in Tables VI and VII. The shift for Ag was studied theoretically before [24]. Our result differs from theirs; this may be due to a simple calculational error in the previous work. Table VI presents separate contributions from the shifts in the ground and excited states. One can see that the disagreement may come from the sign error in a particular contribution. Different signs are caused by energy denominators. For example, when we move from the first to the second line of the table, the sign of the energy denominator for the ground-state contribution changes and so does the contribution itself. Since the other contribution remains the same, the total shift must change.

Table VII shows the second-order Zeeman shift for $^{63}$Cu and $^{197}$Au. As in the case of $^{107}$Ag, the shift is small. Note that Cu has one clock transition with both a tiny quadratic shift coefficient and no linear shift. By measuring two or more $F_{gz} = 0 \to F_{ez} = 0$ Zeeman components and taking appropriate combinations of the corresponding transition frequencies, the second-order shift may be substantially reduced.

The quadratic shift vanishes in the considered approximation for transitions between states with maximum value of $F$ and its projection $F_z$ (see the bottom lines of Table VII). This is because there are no terms in Eq. (17) which would satisfy the selection rules. Note, also, that the (nonzero) numbers in Table VII should be considered as rough estimations only. This is because of uncertainties of the experimental data for the electric quadrupole hfs constant $B$, in particular for Cu [52]. The numbers can change several times depending on which set of data is used.

TABLE VI. Second-order Zeeman shift [mHz/($\mu$T)$^2$] for $^{107}$Ag and comparison with other calculations. The index $g$ is for the ground state and index $c$ is for the excited (clock) state. It is assumed that $F_z = 0$ in both states.

| $F_c$ | $F_g$ | $\Delta E_c/B_0^2$ | $\Delta E_g/B_0^2$ | $(\Delta E_c - \Delta E_g)/B_0^2$ | Ref. [24] |
|---|---|---|---|---|---|
| 2 | 0 | 0.186 | 0.114 | 0.072 | 0.07 |
| 2 | 1 | 0.186 | −0.114 | 0.301 | 0.07 |
| 3 | 1 | −0.186 | −0.114 | −0.072 | −0.3 |

TABLE VII. Second-order Zeeman shift coefficient [mHz/($\mu$T)$^2$] for $^{63}$Cu and $^{197}$Au. Gaps in the data mean that the corresponding set of quantum numbers is not possible for the transition.

| | | | | $(\Delta E_c - \Delta E_g)/B_0^2$ | | |
|---|---|---|---|---|---|---|
| | | | | $^{63}$Cu | $^{63}$Cu | $^{197}$Au |
| $F_g$ | $F_{gz}$ | $F_c$ | $F_{cz}$ | $^2D_{5/2}$ | $^2D_{3/2}$ | $^2D_{5/2}$ |
| 1 | 0 | 0 | 0 | | −0.759 | |
| 1 | 0 | 1 | 0 | 0.087 | 0.743 | 0.023 |
| 1 | 0 | 2 | 0 | 0.193 | 0.058 | 0.027 |
| 1 | 0 | 3 | 0 | −0.247 | 0.025 | 0.050 |
| 2 | 0 | 0 | 0 | | −0.792 | |
| 2 | 0 | 1 | 0 | 0.053 | 0.710 | −0.041 |
| 2 | 0 | 2 | 0 | 0.160 | 0.024 | −0.037 |
| 2 | 0 | 3 | 0 | −0.281 | −0.009 | −0.014 |
| 2 | 0 | 4 | 0 | 0.001 | | −0.037 |
| 2 | ±2 | 3 | ±2 | −0.044 | 0.004 | 0.002 |
| 2 | ±2 | 3 | ±3 | −0.017 | 0.0 | 0.004 |
| 2 | ±2 | 4 | ±4 | 0.0 | | 0.0 |

## IV. SEARCH FOR NEW PHYSICS

An exceptionally high accuracy of atomic clocks is a great advantage for using them in a search for new physics. The search is conducted by monitoring relative values of different atomic frequencies over a significant time interval. Establishing a time variation of the frequency ratio allows multiple interpretations. For example, the interaction between low-mass scalar dark matter and ordinary matter may lead to oscillation of the fine-structure constant and a transient variation effect [58–60]. In this section, we consider the sensitivities to a hypothetical time variation of the fine-structure constant, $\alpha$ ($\alpha = e^2/\hbar c$), to local position invariance (LPI) violation, and to local Lorentz invariance (LLI) violation.

### A. Time variation of the fine-structure constant

It is convenient to parametrize the $\alpha$ dependence of atomic frequencies by the formula $\omega = \omega_0 + q[(\frac{\alpha}{\alpha_0})^2 - 1]$ [8], where $\alpha_0$ and $\omega_0$ are present-day values of the fine-structure constant and the frequency of the transition, and $q$ is the sensitivity coefficient, which comes from the calculations. To monitor a possible frequency change with time, one atomic frequency is measured against another. Then,

$$\frac{\partial}{\partial t} \ln \frac{\omega_1}{\omega_2} = \frac{\dot{\omega}_1}{\omega_1} - \frac{\dot{\omega}_2}{\omega_2} = \left(\frac{2q_1}{\omega_1} - \frac{2q_2}{\omega_2}\right)\frac{\dot{\alpha}}{\alpha}. \tag{18}$$

The value $K = 2q/\omega$ is called an enhancement factor. It shows that if $\alpha$ changes in time, then $\omega$ changes $K$ times faster. Calculated values of $q$ and $K$ for different optical clock transitions are presented in Table VIII. We include all clock transitions of the present work and those transitions of previously studied clocks, which are sensitive to $\alpha$ variation. We remark that work on the historically important $Hg^+$ ion clock [9,17] has been stopped. We nevertheless include it in the discussion. There are seven transitions where $|K| > 1$. The largest values of $|K|$ correspond to the smallest values of transition frequency $\omega$. It would be wrong to say that all these transitions

TABLE VIII. Sensitivity of clock transitions to variation of the fine-structure constant ($q, K$), to LLI violation [reduced matrix element $\langle c||T_0^{(2)}||c\rangle$ of the tensor operator (22) for the upper state $c$], and to LPI violation (relativistic factor $R$). Note that $\langle g||T_0^{(2)}||g\rangle$ is zero for the ground state of all clocks due to the small value of the total angular momentum $J \leqslant 1/2$.

| Atom/ | Transition | | | $\hbar\omega$[a] | $q$ | | $\langle c\|\|T_0^{(2)}\|\|c\rangle$ | $R$ | |
|---|---|---|---|---|---|---|---|---|---|
| Ion | Lower state | | Upper state | ($\mathrm{cm}^{-1}$) | ($\mathrm{cm}^{-1}$) | $K = 2q/\hbar\omega$ | (a.u.) | Present | Other |
| Cu | $3d^{10}4s\ ^2S_{1/2}$ | – | $3d^94s^2\ ^2D_{5/2}$ | 11202.565 | −4000 | −0.71 | −48 | 0.98 | |
| Cu | $3d^{10}4s\ ^2S_{1/2}$ | – | $3d^94s^2\ ^2D_{3/2}$ | 13245.443 | −1900 | −0.29 | −37 | 0.99 | |
| Cu | $3d^94s^2\ ^2D_{5/2}$ | – | $3d^94s4p\ ^4F^o_{9/2}$ | 29706.54 | 2100 | 0.14 | −48 | | |
| Ag | $4d^{10}5s\ ^2S_{1/2}$ | – | $4d^95s^2\ ^2D_{5/2}$ | 30242.061 | −11300 | −0.75 | −41 | 0.93 | |
| Au | $5d^{10}6s\ ^2S_{1/2}$ | – | $5d^96s^2\ ^2D_{5/2}$ | 9161.177 | −38550 | −8.4 | −45 | 0.67 | |
| Au | $5d^96s\ ^2D_{5/2}$ | – | $5d^96s6p\ ^4F^o_{9/2}$ | 39535.970 | 24200 | 1.2 | −44 | | |
| Yb[c] | $4f^{14}6s^2\ ^1S_0$ | – | $4f^{14}6s6p\ ^3P^o_0$ | 17288.439 | 2714 | 0.31 | 0 | 1.12 | 1.20[b] |
| Yb[c] | $4f^{14}6s^2\ ^1S_0$ | – | $4f^{13}5d6s^2 J=2$ | 23188.518 | −44290 | −3.82 | −72[d] | 0.65 | 1.40[e] |
| Yb[e] | $4f^{14}6s6p\ ^1P^o_0$ | – | $4f^{13}5d6s^2 J=2$ | 5900.079 | −43530 | −15 | −72[d] | | |
| Yb II[f] | $4f^{14}6s\ ^2S_{1/2}$ | – | $4f^{13}6s^2\ ^2F^o_{7/2}$ | 21418.75 | −56737 | −5.3 | −135 | 0.58 | −1.90[b] |
| Yb II[f] | $4f^{14}6s\ ^2S_{1/2}$ | – | $4f^{14}5d\ ^2D_{3/2}$ | 22960.80 | 10118 | 0.88 | 10[d] | 1.42 | 1.48[b] |
| Yb II[e] | $4f^{13}6s^2\ ^2F^o_{7/2}$ | – | $4f^{14}5d\ ^2D_{3/2}$ | 1542.06 | −66855 | −87 | 10[d] | | |
| Hg II[g] | $5d^{10}6s\ ^2S_{1/2}$ | – | $5d^96s^2\ ^2D_{5/2}$ | 35514.624 | −52200 | −2.94 | | 0.68 | 0.2[b] |

[a]NIST [53].
[b]Reference [9].
[c]Reference [19].
[d]Present work.
[e]Reference [61].
[f]References [11,56].
[g]References [8,19].

are good for searching for $\alpha$ variation. This is because the accuracy of the measurements is equally important (see, also, the discussion in Ref. [19]). The true figure of merit is the ratio of the relative frequency shift due to variation of $\alpha$ and the fractional uncertainty of the measurements, $(q/\omega)/(\delta\omega/\omega) = q/\delta\omega$. This ratio does not (directly) depend on $\omega$. Therefore, looking for a large value of $K$ caused by the small value of $\omega$ brings no benefit. The value of the relativistic energy shift $q$ is more important. Comparing the values of $q$ for different clock transitions (see Table VIII), we see that the $E2$ clock transition sensitivity for Au is essentially as large as the recently proposed new transitions in neutral ytterbium [19] and only 30% smaller than the octupole transition in the ytterbium ion (Yb II). It is possible to search for $\alpha$ variation by comparing two clock transitions in the same atom, i.e., gold. The corresponding differential sensitivity factor is $q_{2-7} - q_{1-2} \simeq 63 \times 10^3\ \mathrm{cm}^{-1}$. This value is similar to the differential sensitivity of the two clock transitions in the ytterbium ion.

### B. LPI violation

In the standard model extension, the term in the Hamiltonian responsible for the LPI violation can be presented in the form (see, e.g., Ref. [9])

$$\hat{H}_{\mathrm{LPI}} = c_{00}\frac{2}{3}\frac{U}{c^2}\hat{K}, \tag{19}$$

where $c_{00}$ is the unknown parameter characterizing the magnitude of the LPI violation, $U$ is the gravitational potential, $c$ is the speed of light, $\hat{K} = c\gamma_0\gamma^j p_j/2$ is the relativistic operator of kinetic energy, in which $\gamma_0$ and $\gamma^j$ are Dirac matrices, and $\mathbf{p} = -i\hbar\boldsymbol{\nabla}$ is the electron momentum operator.

The presence of the term (19) in the Hamiltonian would manifest itself via a dependence of the atomic frequencies on the time of the year, caused by the changing Sun-Earth distance leading to a change of the Sun's gravitational potential $U$. As in the case of the $\alpha$ variation, at least two clock transitions are needed to measure one clock frequency against the other. The interpretation of the measurements is based on the formula [9]

$$\frac{\Delta\omega_1}{\omega_1} - \frac{\Delta\omega_2}{\omega_2} = -(R_1 - R_2)\frac{2}{3}c_{00}\frac{\Delta U}{c^2}, \tag{20}$$

where $\Delta\omega$ and $\Delta U$ are the change of atomic frequencies and gravitational potential between the measurements, respectively. $R$ in Eq. (20) is the relativistic factor, which describes the deviation of the kinetic energy $E_K$ from the value given by the nonrelativistic virial theorem (which states that $E_K = -E$, where $E$ is the total energy),

$$R_{ab} = -\frac{E_{K,a} - E_{K,b}}{E_a - E_b}. \tag{21}$$

The values of the factor $R$ are calculated in computer codes by varying the value of the kinetic-energy operator in the Dirac equation (see Ref. [9] for details).

The results are very sensitive to the many-body effects, which means that the effects should be treated very accurately or avoided. Otherwise, the results are unstable. A good criterion for the reliability of the results is the achievement of the nonrelativistic limit $R = 1$. This can be done by setting to zero the value of the fine-structure constant $\alpha$ in the computer codes. It turns out that for complicated systems

such as those considered in the present work, the best results are obtained by simple estimations based on single-electron consideration. Namely, the clock transitions in Cu, Ag, and Au can be considered as $ns \to (n-1)d_{5/2}$ single-electron transitions ($n = 4, 5, 6$ for Cu, Ag, and Au, respectively). Therefore, we just use single-electron energies of theses states in Eq. (21). We use the same approach for $Hg^+$ and $Yb^+$.

The results are presented in Table VIII, together with the results obtained earlier for other systems. Note that the results for the transitions involving excitation from the $5d$ shell in $Hg^+$ and the $4f$ shell in $Yb^+$ are different from what was published before. The old calculations were based on a version of the CI method [62,63] that contained a fitting parameter responsible for the correct energy interval between states of different configurations. It was assumed that this parameter does not change under variation of the kinetic-energy operator. We believe that the present results are more reliable because they are free from any assumptions and because they reproduce the nonrelativistic limit $R = 1$. Note that the values of $R$ for transitions in Yb and $Yb^+$, which do not involve excitation from the $4f$ shell, are in good agreement with previous calculations ($R = 1.12$ and $R = 1.42$; see Table VIII). This means that the present single-electron estimations work well and that accurate many-body calculations are possible for simple systems.

To study the LPI violation, one needs to compare two clocks with different values of the relativistic factors $R$ [see formula (20)] over at least half of a year. An important past experiment with optical clocks was the comparison of a $Hg^+$ clock with an $Al^+$ clock [9,17]. Table VIII shows that there are various choices for such clock pairs. In particular, the Au clock's sensitivity is comparatively strong (with a large negative deviation from the nonrelativistic value $R = 1$). Thus, it is suitable for pairing with a clock with strong, but opposite sensitivity, such as the standard Yb lattice clock ($R > 1$). It is more sensitive than the Cu-Yb pairing by a factor 2.5. The two clock transitions in $Yb^+$ have the largest difference $|R_1 - R_2|$.

### C. LLI violation

The LLI violation term is a tensor operator,

$$\hat{H}_{\rm LLI} = -\tfrac{1}{6} C_0^{(2)} T_0^{(2)}, \tag{22}$$

where $C_0^{(2)}$ is unknown constant and the relativistic form of the $T_0^{(2)}$ operator is given by $T_0^{(2)} = c\gamma_0(\gamma^j p_j - 3\gamma^3 p_3)$. To study the effect of the LLI violating term (22), one needs long-lived atomic states with a large value of the total electron angular momentum $J$, $J > 1/2$. All clock states of Cu, Ag, and Au satisfy this requirement. Note that the established lattice optical clocks Yb, Sr, and Hg do not satisfy this requirement and are thus not suitable for testing LLI.

The term (22) should cause a dependence of the atomic frequencies on the apparatus orientation in space (e.g., due to Earth rotation). Interpretation of the measurements requires knowing the values of the reduced matrix elements of the operator $T_0^{(2)}$ for the clock states. We calculate these matrix elements using the CIPT method to obtain wave functions and the RPA method to obtain the effective operator for valence electrons.

The results are presented in Table VIII. The results of earlier calculations for Yb II [11] are also presented for comparison. In contrast to the search of the $\alpha$ variation and LPI violation, one clock state is sufficient for the search of the LLI violation. The comparison of frequencies is done for states with different projections of the total angular momentum $J$ [10,11].

The large value of the matrix element is important, but it is not the most important parameter, e.g., the lifetime of the metastable state is even more important (see, e.g., [11] for more discussion). Obviously, in addition, the uncertainty of the clock is also crucial. The calculations show that Cu, Ag, and Au are suitable for the search for LLI violation.

## V. CONCLUSION

We further advanced the CIPT method of electronic structure calculations for atoms with open shells by calculating the correction to the wave function caused by mixing with high-energy states. We used this method to study electric quadrupole transitions between ground and excited metastable states of Cu, Ag, and Au and demonstrated that the transitions have important features of optical clock transitions.

A main result of this work is that we have identified three elements for which the blackbody shift is smaller than that of the standard lattice clocks (notably strontium) by a factor of up to approximately 100. The predicted shifts for Ag and Au are also smaller than the predicted shifts in Cd, Zn, and Yb (431 nm). At present, among the neutral species, only Tm has a smaller (measured) blackbody shift [64].

Other sensitivities to external perturbing fields, such as Zeeman and Stark sensitivities, are similar to or smaller than that in current top-performing optical clocks and lead to well-controllable shifts. These results lead to the identification of Ag and Au as two particularly valuable candidates for next-generation optical lattice clocks.

We remark that as an example, the laser system required for Au is commercially available and does not require particularly difficult deep-ultraviolet wavelengths. For example, the 268 nm cooling wavelength of Au can be easily obtained as the fourth harmonic of a powerful $Yb^+$-doped fiber laser at 1071 nm. The narrow-linewidth cooling requires a laser, e.g., at 456 nm, which is a wavelength available from a diode laser. The clock laser radiation can be directly provided by a fiber laser.

Analyzing the performance of the new clock transitions for the search for physics beyond the standard model, we find neutral atom clock candidates that have a nonzero and relevant sensitivity to violations of local Lorentz invariance. Our finding includes the recently proposed additional clock transition of Yb (431 nm). Such tests do not require a second atomic clock.

We furthermore found that the pairing of the Au clock with the already established Yb lattice clock (578 nm transition) would be a particularly sensitive choice for a test of local position invariance as reflected in the difference of $R$ factors.

Finally, we had previously found that the 1092 nm transition of Au also exhibits a strong sensitivity to variation of $\alpha$. The sensitivity $K$ is approximately 27 times larger than for the standard Yb lattice clock, so that a pairing with the latter

represents an option. Alternatively, the search for $\alpha$ variation can be done by pairing two clock transitions in the Au atom. The sensitivity coefficients $q$ in the two Au clock transitions have opposite sign and this doubles the overall sensitivity to variation of $\alpha$. Note that this is only the second neutral atomic species found (besides Yb) that exhibits this feature. Thus, there now exist concrete options for lattice-clock-based tests of $\alpha$ variation.

A reevaluation of the relativistic factor $R$ of four clock transitions in Yb, $Yb^+$, and $Hg^+$ has led to significant changes in the values. Use of the correct values is crucial to derive the correct upper bounds for local position invariance violation, and also for selection of suitable clock pairs in future experimental campaigns.

We emphasize that these sensitivities are to be considered together with the eventually achievable accuracy and long-term stability of the clock frequencies. It is for these reasons that we have studied some important systematic shifts here. Because of the potential of the Cu, Ag, and Au clock, our work provides a strong motivation for experimental studies of their blackbody radiation shifts and lattice-induced shifts.

## ACKNOWLEDGMENTS

We thank one referee for pointing out Ref. [34] to us. This work was supported by the National Natural Science Foundation of China (Grant No. 11874090) and the Australian Research Council (Grants No. DP190100974 and No. DP200100150). V.A.D. would like to express special thanks to the Institute of Applied Physics and Computational Mathematics in Beijing for its hospitality and support. The work of S.S. was performed in the framework of Project No. Schi 431/22-1 of the Deutsche Forschungsgemeinschaft. This research includes computations using the computational cluster Katana supported by Research Technology Services at UNSW Sydney.

## APPENDIX A: STARK AND ELECTRIC QUADRUPOLE SHIFTS

The Stark shift of the frequency of the transition between atomic states $a$ and $b$ due to interaction with residual static electric field $\varepsilon$ is

$$\delta\omega_{ab} = -\Delta\alpha_{ab}(0)\left(\frac{\varepsilon}{2}\right)^2, \tag{A1}$$

where $\Delta\alpha_{ab}(0)$ is the difference between the static scalar polarizabilities of states $a$ and $b$. The shift is quadratic in the electric field and usually small. It is further suppressed for the considered clock transitions due to the small difference in the polarizabilities (see Table IV).

The energy shift due to a gradient of a residual static electric field $\varepsilon$ is described by a corresponding term in the Hamiltonian

$$\hat{H}_Q = -\frac{1}{2}\hat{Q}\frac{\partial\varepsilon_z}{\partial z}, \tag{A2}$$

where $\hat{Q}$ is the atomic quadrupole moment operator ($\hat{Q} = |e|r^2Y_{2m}$, which is the same as for the $E2$ transitions). The energy shift of a state with total angular momentum $J$ is proportional to the atomic quadrupole moment of this state. It is defined as twice the expectation value of the $\hat{Q}$ operator in the stretched state,

$$Q_J = 2\langle J, J_z = J|\hat{Q}|J, J_z = J\rangle. \tag{A3}$$

Calculations using the CIPT method for wave functions and the RPA method for the operator give the values $Q_J = 0.431$ a.u. for the $^2D_{5/2}$ clock state of Cu, $Q_J = 0.296$ a.u. for the $^2D_{3/2}$ clock state of Cu, $Q_J = 0.966$ a.u. for the clock state of Ag, and $Q_J = 1.47$ a.u. for the clock state of Au. The quadrupole moments of the ground states of these atoms are zero due to the small value of the total electron angular momentum ($J = 1/2$).

Consider transitions between hyperfine-structure (hfs) components of the ground and clock states with definite values of the total angular momentum $F$. The quadrupole shift is given by

$$\Delta E_Q = \frac{F_z^2 - F(F+1)}{2F(2F-1)}Q\frac{\partial\varepsilon_z}{\partial z}, \tag{A4}$$

where $F_z$ is the projection of $F$. For $F = 3$ and $F_z = \pm 2$, the shift is zero. Note that clock states with $F = 3$ exist for all stable isotopes of all three considered atoms (see Table IX). Using these states would lead to a linear Zeeman shift. It cancels out by averaging over the transition frequencies to the states with $F_z = -2$ and $F_z = 2$. For $F_z \neq \pm 2$, the estimations can be done in the following way. On the inner surface of a metallic vacuum chamber, there can be spatial variations of the electrostatic potential of the order of 0.1 V. The typical internal size of a vacuum chamber may be 10 cm. The corresponding Stark shift is $\sim 10^{-7}$ Hz. The electric-field gradient is smaller than 0.1 V/(10 cm)$^2$. Considering that the factor before the electric-field gradient in Eq. (A4) is $\sim$1 a.u. leads to a negligible quadrupole shift of $\sim 10^{-5}$ Hz.

TABLE IX. Stable isotopes with nonzero nuclear spin ($I$) and possible values of total angular momentum $F$ ($\mathbf{F} = \mathbf{I} + \mathbf{J}$) for ground states (GS) and clock states (CS) of Cu, Ag, and Au.

| Isotopes | Transition | $I$ | $F$ for GS | $F$ for CS |
|---|---|---|---|---|
| $^{63,65}$Cu, $^{197}$Au | $^2S_{1/2} - {}^2D_{5/2}$ | 3/2 | 1,2 | 1,2,3,4 |
| $^{63,65}$Cu | $^2S_{1/2} - {}^2D_{3/2}$ | 3/2 | 1,2 | 0,1,2,3 |
| $^{107,109}$Ag | $^2S_{1/2} - {}^2D_{5/2}$ | 1/2 | 0,1 | 2,3 |

## APPENDIX B: HYPERFINE STRUCTURE

The atoms considered here all exhibit hyperfine structure in the ground state, in the clock state, and in the excited state addressed in laser cooling. The nuclear spins are given in Table IX. The hfs splitting is approximately given by [45]

$$E_{\rm hfs}(F) = \frac{A}{2}F(F+1) + \frac{B}{2}\{F^2(F+1)^2 + F(F+1)[1 - 2J(J+1) - 2I(I+1)]\}. \tag{B1}$$

The total angular momentum is $\mathbf{F} = \mathbf{J} + \mathbf{I}$, where $I$ is nuclear spin. $A$ and $B$ are magnetic dipole and electric quadrupole hfs constants, respectively. They are reported in Table V. In addition, for $I = 3/2$ nuclei, there is a small octupole hfs contribution [22,23].

For example, the hyperfine structure of Au was studied experimentally with high precision in the 1960s, and was also calculated [54,55]. The hyperfine splitting between $F = 1, 2$ in the ground state amounts to 6.10 GHz [57]. The splittings in $^2D_{5/2}$ are [22]

$F = 1 \leftrightarrow F = 2$: 1.00 GHz,
$F = 2 \leftrightarrow F = 3$: 0.71 GHz, and
$F = 3 \leftrightarrow F = 4$: 0.52 GHz.

The splittings in $^2D_{3/2}$ are [23]

$F = 0 \leftrightarrow F = 1$: 1.11 GHz,
$F = 1 \leftrightarrow F = 2$: 1.31 GHz, and
$F = 2 \leftrightarrow F = 3$: 0.31 GHz.

The hfs in the $^4F$ state has also been studied experimentally [23]. We show these numbers to indicate to experimentalists that one will need to use appropriate repumping lasers or modulators.


[1] A. D. Ludlow, M. M. Boyd, J. Ye, E. Peik, and P. O. Schmidt, Rev. Mod. Phys. **87**, 637 (2015).
[2] C. W. Chou, D. B. Hume, J. C. J. Koelemeij, D. J. Wineland, and T. Rosenband, Phys. Rev. Lett. **104**, 070802 (2010).
[3] N. Hinkley, J. A. Sherman, N. B. Phillips, M. Schioppo, N. D. Lemke, K. Beloy, M. Pizzocaro, C. W. Oates, and A. D. Ludlow, Science **341**, 1215 (2013).
[4] K. Beloy, N. Hinkley, N. B. Phillips, J. A. Sherman, M. Schioppo, J. Lehman, A. Feldman, L. M. Hanssen, C. W. Oates, and A. D. Ludlow, Phys. Rev. Lett. **113**, 260801 (2014).
[5] I. Ushijima, M. Takamoto, M. Das, T. Ohkubo, and H. Katori, Nat. Photon. **9**, 185 (2015).
[6] T. L. Nicholson, S. L. Campbell, R. B. Hutson, G. E. Marti, B. J. Bloom, R. L. McNally, W. Zhang, M. D. Barrett, M. S. Safronova, G. F. Strouse, W. L. Tew, and J. Ye, Nat. Commun. **6**, 6896 (2015).
[7] N. Nemitz, T. Ohkubo, M. Takamoto, I. Ushijima, M. Das, N. Ohmae, and H. Katori, Nat. Photon. **10**, 258 (2016).
[8] V. V. Flambaum and V. A. Dzuba, Can. J. Phys. **87**, 25 (2009).
[9] V. A. Dzuba and V. V. Flambaum, Phys. Rev. D **95**, 015019 (2017).
[10] R. Shaniv, R. Ozeri, M. S. Safronova, S. G. Porsev, V. A. Dzuba, V. V. Flambaum, and H. Häffner, Phys. Rev. Lett. **120**, 103202 (2018).
[11] V. A. Dzuba, V. V. Flambaum, M. S. Safronova, S. G. Porsev, T. Pruttivarasin, M. A. Hohensee, and H. Häffner, Nat. Phys. **12**, 465 (2016).
[12] S. Schiller, Phys. Rev. Lett. **98**, 180801 (2007).
[13] J. C. Berengut, V. A. Dzuba, and V. V. Flambaum, Phys. Rev. Lett. **105**, 120801 (2010).
[14] J. C. Berengut, V. A. Dzuba, V. V. Flambaum, and A. Ong, Phys. Rev. A **86**, 022517 (2012).
[15] V. A. Dzuba and V. V. Flambaum, Hyperfine Interact. **236**, 79 (2015).
[16] C. J. Campbell, A. G. Radnaev, A. Kuzmich, V. A. Dzuba, V. V. Flambaum, and A. Derevianko, Phys. Rev. Lett. **108**, 120802 (2012).
[17] T. Rosenband, D. B. Hume, P. O. Schmidt, C. W. Chou, A. Brusch, L. Lorini, W. H. Oskay, R. E. Drullinger, T. M. Fortier, J. E. Stalnaker, S. A. Diddams, W. C. Swann, N. R. Newbury, W. M. Itano, D. J. Wineland, and J. C. Bergquist, Science **319**, 1808 (2008).
[18] Z. Xiang, L. Ben-Quan, L. Ji-Guang, and Z. Hong-Xin, Acta Phys. Sin. **68**, 043101 (2019).
[19] V. A. Dzuba, V. V. Flambaum, and S. Schiller, Phys. Rev. A **98**, 022501 (2018).
[20] C. Sanner, N. Huntemann, R. Lange, C. Tamm, E. Peik, M. S. Safronova, and S. G. Porsev, Nature (London) **567**, 204 (2019).
[21] V. A. Dzuba, V. V. Flambaum, and J. K. Webb, Phys. Rev. A **59**, 230 (1999).
[22] W. J. Childs and L. S. Goodman, Phys. Rev. **141**, 176 (1966).
[23] A. G. Blachman, D. A. Landman, and A. Lurio, Phys. Rev. **161**, 60 (1967)
[24] T. Badr, M. D. Plimmer, P. Juncar, M. E. Himbert, Y. Louyer, and D. J. E. Knight, Phys. Rev. A **74**, 062509 (2006).
[25] V. A. Dzuba, J. C. Berengut, C. Harabati, and V. V. Flambaum, Phys. Rev. A **95**, 012503 (2017).
[26] F. A. Parpia, C. F. Fischer, and I. P. Grant, Comput. Phys. Commun. **94**, 249 (1996).
[27] B. G. C. Lackenby, V. A. Dzuba, and V. V. Flambaum, Phys. Rev. A **98**, 022518 (2018).
[28] B. G. C. Lackenby, V. A. Dzuba, and V. V. Flambaum, Phys. Rev. A **99**, 042509 (2019).
[29] B. G. C. Lackenby, V. A. Dzuba, and V. V. Flambaum, Phys. Rev. A **98**, 042512 (2018).
[30] J. Li and V. Dzuba, J. Quantum Spectrosc. Radiat. Transfer **247**, 106943 (2020).
[31] S. O. Allehabi, J. Li, V. A. Dzuba, and V. V. Flambaum, J. Quantum Spectrosc. Radiat. Transfer **253**, 107137 (2020).
[32] W. R. Johnson and J. Sapirstein, Phys. Rev. Lett. **57**, 1126 (1986).
[33] V. A. Dzuba, V. V. Flambaum, P. G. Silvestrov, and O. P. Sushkov, J. Phys. B **20**, 1399 (1987).
[34] R. Kurucz, Kurucz's Atomic Database, http://kurucz.harvard.edu/atoms/2900/lifemeta2900.dat and http://kurucz.harvard.edu/atoms/4700/gf4700.gam.
[35] P. Hannaford, P. L. Larkins, and R. M. Lowe, J. Phys. B **14**, 2321 (1981).
[36] J. Carlsson, P. Jönsson, and L. Sturesson, Z. Phys. D **16**, 87 (1990).
[37] P. L. Larkins and P. Hannaford, Z. Phys. D **32**, 167 (1994).
[38] T. Badr, M. D. Plimmer, P. Juncar, M. E. Himbert, J. D. Silver, and G. D. Rovera, Eur. Phys. J. D **31**, 3 (2004).
[39] P. S. Doidge, Spectrochim. Acta, Part B **50**, 209 (1995); **50**, 1421 (1995); **51**, 375 (1996).
[40] M. Kock and J. Richter, Z. Astrophys. **69**, 180 (1968).
[41] W. L. Wiese and G. A. Martin, in *Wavelengths and Transition Probabilities for Atoms and Atomic Ions*, Natl. Stand. Ref. Data Ser. No. NSRDS-68 (Natl. Bureau of Standards, Washington, D.C., 1980), pp. 359–406.
[42] G. Uhlenberg, J. Dirscherl, and H. Walther, Phys. Rev. A **62**, 063404 (2000).
[43] N. Brahms, B. Newman, C. Johnson, T. Greytak, D. Kleppner, and J. Doyle, Phys. Rev. Lett. **101**, 103002 (2008).

[44] P. Schwerdtfeger and J. K. Nagle, Mol. Phys. **117**, 1200 (2019).
[45] L. D. Landau and E. M. Lifshitz, *Quantum Mechanics. Non-relativistic Theory*, 2nd ed. (Pergamon, Oxford, 1965).
[46] V. A. Dzuba, A. Kozlov, and V. V. Flambaum, Phys. Rev. A **89**, 042507 (2014).
[47] V. A. Dzuba, V. V. Flambaum, and M. G. Kozlov, Phys. Rev. A **54**, 3948 (1996).
[48] S. G. Porsev and A. Derevianko, Phys. Rev. A **74**, 020502(R) (2006); **86**, 029904(E) (2012).
[49] T. Middelmann, S. Falke, C. Lisdat, and U. Sterr, Phys. Rev. Lett. **109**, 263004 (2012).
[50] J. A. Sherman, N. D. Lemke, N. Hinkley, M. Pizzocaro, R. W. Fox, A. D. Ludlow, and C. W. Oates, Phys. Rev. Lett. **108**, 153002 (2012)
[51] J. Tenenbaum, I. Smilanski, S. Gabay, L. A. Levin, G. Erez, and S. Lavi, Opt. Commun. **32**, 473 (1980).
[52] B. K. Ankush and M. N. Deo, J. Quantum Spectrosc. Radiat. Transfer **134**, 21 (2014).
[53] A. Kramida, Yu. Ralchenko, J. Reader, and NIST ASD Team (2018), NIST Atomic Spectra Database (ver. 5.5.2), https://physics.nist.gov/asd (National Institute of Standards and Technology, Gaithersburg, MD, 2018).
[54] W. M. Itano, J. Res. Natl. Inst. Stand. Technol. **105**, 829 (2000).
[55] J. Bieroń, C. Froese Fischer, P. Indelicato, P. Jönsson, and P. Pyykkö, Phys. Rev. A **79**, 052502 (2009).
[56] V. A. Dzuba, V. V. Flambaum, and M. V. Marchenko, Phys. Rev. A **68**, 022506 (2003).
[57] H. Dahmen and S. Penselin, Z. Phys. **200**, 456 (1967).
[58] A. Arvanitaki, J. Huang, and K. Van Tilburg, Phys. Rev. D **91**, 015015 (2015).
[59] K. Van Tilburg, N. Leefer, L. Bougas, and D. Budker, Phys. Rev. Lett. **115**, 011802 (2015).
[60] Y. V. Stadnik and V. V. Flambaum, Phys. Rev. Lett. **115**, 201301 (2015).
[61] M. S. Safronova, S. G. Porsev, C. Sanner, and J. Ye, Phys. Rev. Lett. **120**, 173001 (2018).
[62] V. A. Dzuba and V. V. Flambaum, Phys. Rev. A **77**, 012514 (2008).
[63] V. A. Dzuba and V. V. Flambaum, Phys. Rev. A **77**, 012515 (2008).
[64] A. Golovizin, E. Fedorova, D. Tregubov, D. Sukachev, K. Khabarova, V. Sorokin, and N. Kolachevsky, Nat. Commun. **10**, 1724 (2019).
[65] Y. Ting and H. Lew, Phys. Rev. **105**, 581 (1957).